JOURNAL OF AERONAUTICS AND SPACE TECHNOLOGIES
JANUARY 2005 VOLUME 2 NUMBER 1 (47-55)

NUMERICAL SOLUTION OF THE EULER EQUATIONS BY FINITE VOLUME METHODS: Central versus Upwind Schemes

Murat UYGUN
Hava Harp Okulu
Yeşilyurt-İSTANBUL
muygun@hho.edu.tr

Kadir KIRKKÖPRÜ
İTÜ Makina Fakültesi
Gümüşsuyu- İSTANBUL
kirkkopruk@itu.edu.tr

ABSTRACT

Euler equations are solved by means of three efficient and robust finite volume schemes, namely, central scheme of Jameson-Schmidt-Turkel (JST) and upwind schemes of Roe's Approximate Riemann Solver and Convective Upwind Split Pressure (CUSP) Scheme. Cell-centered discretization technique is employed. Multistage time-stepping algorithm is used to advance the solution in time. Acceleration techniques including local time stepping and implicit residual smoothing are applied for faster convergence to steady state. The flux at the cell faces is computed using MUSCL approach in upwind schemes and simple averaging procedure in JST scheme. MUSCL is enhanced by employing Van Albada limiter to suppress oscillations in regions of sharp gradients. Attention is directed towards the accuracy, convergence, and computational performance of the schemes. All schemes yield good convergence rates for a wide range of flow speeds.

Keywords: *Euler Equations, Central and Upwind Schemes, Multistage Time-stepping, Acceleration Techniques, MUSCL Approach.*

1. INTRODUCTION:

Computational Fluid Dynamics (CFD) has been accepted as an efficient tool in mechanical and aeronautical engineering community and design engineers are running various CFD codes in order to predict the performance of their designs. Due to being an active player on the scene of engineering design, the strong need grows to assess the accuracy and efficiency of the CFD algorithms for inviscid and viscous flows.

Navier-Stokes equations govern the flows of viscous, heat-conducting fluids. In the limit of vanishing dissipation terms ($Re \to \infty$), Euler equations governing the flows of inviscid, adiabatic fluids are resulted. Due to exclusion of the diffusive effects, the applicability of the Euler equations for real flow simulations is limited. However, the dominating convective character of most flow situations at high Reynolds numbers advocates the importance of their accurate numerical simulation. Most methods used for discretization of convective part of the Navier-Stokes equations are same as the methods based on Euler equations. Also, the difficulties with discretization and solution procedure regarding the non-linear convective terms, are kept in Euler equations. Hence, development of an Euler solver is of great importance for the construction of a Navier-Stokes solver. Solutions of Euler equations are needed for various reasons such as for providing unique shock solutions for flows in converging-diverging ducts, for determining the rotational flowfield behind a shock past a wing or nacelle, etc. With its current position, Euler solvers are widely used in a variety of applications for flows with complex geometries.

In the current work, two dimensional Euler solver based on cell-centered finite volume discretization technique was studied. Use of conservation form of the governing equation in finite volume discretization technique allows the shock waves to be captured as weak solutions to the governing equations and application of shock-fitting techniques is not needed further. Convective terms were evaluated using central scheme of JST [1], and upwind schemes of Roe's approximate Riemann solver [2] and CUSP scheme [3]. Upwind schemes, in which discretization is based on the characteristics of Euler equations, have the advantage of being naturally dissipative. Separate dissipation terms are added in central schemes to overcome oscillations arising in regions of strong gradients. An explicit second-order accurate upwind scheme can also have twice the stability bound of a second-order scheme [4]. In the cell-centered scheme, the flow variables are located at the cell centers. The

flux vectors at the midpoint of a cell face are computed by simple averaging of flow variables at two neighboring cells in central scheme whereas two flow variables named "the left and the right state," which are interpolated from left and right side of the cell face using a non-symmetric formulae are utilized in upwind schemes. A famous choice for interpolation, which is known as Monotone Upwind Schemes for Scalar Conservation Laws (MUSCL) was used [5]. MUSCL was enhanced by using Van Albada Limiter [6] in order to suppress the non-physical oscillations of the solution near the regions of strong flow gradients. Time integration to steady state was done by using five stage hybrid schemes, in which dissipation terms can be evaluated at odd stages only to decrease the computational work and are blended to increase the stability of the scheme. However, the convergence of the basic scheme slows down considerably due to time step limitation associated with the small mesh cells. This disadvantage was overcome by applying two acceleration techniques such as local time-stepping and implicit residual smoothing.

2. GOVERNING EQUATIONS:

The integral form of the Navier-Stokes equations can be written as

$$\frac{\partial}{\partial t}\int_{\Omega}\vec{W}d\Omega+\oint_{\partial\Omega}\left(\vec{F}_c-\vec{F}_v\right)dS=\int_{\Omega}\vec{Q}d\Omega \qquad (1)$$

where $\vec{W}$, $\vec{F}_C$, $\vec{F}_V$, and $\vec{Q}$ are the vectors of conservative variables, convective and diffusive fluxes, and source terms:

$$\vec{W}=\begin{bmatrix}\rho\\ \rho u\\ \rho v\\ \rho E\end{bmatrix} \qquad \vec{F}_v=\begin{bmatrix}0\\ n_x\tau_{xx}+n_y\tau_{xy}+n_z\tau_{xz}\\ n_x\tau_{yx}+n_y\tau_{yy}+n_z\tau_{yz}\\ n_x\Theta_x+n_y\Theta_y+n_z\Theta_z\end{bmatrix}$$

$$\vec{F}_c=\begin{bmatrix}\rho V\\ \rho uV+n_x p\\ \rho vV+n_y p\\ \rho HV\end{bmatrix} \qquad \vec{Q}=\begin{bmatrix}0\\ \rho f_{e,x}\\ \rho f_{e,y}\\ \rho\vec{f}_e\cdot\vec{v}+\dot{q}_h\end{bmatrix} \qquad (2)$$

with the contravariant velocity V defined as

$$V=\vec{v}\cdot\vec{n}=n_x u+n_y v. \qquad (3)$$

For flows of inviscid, adiabatic fluids, $\vec{F}_V=0$, and Euler equations are resulted. Source terms are assumed to be negligible $\vec{Q}\approx 0$. The total enthalpy H is computed as

$$H=h+\frac{|\vec{v}|^2}{2}=E+\frac{p}{\rho} \qquad (4)$$

Assuming air as an ideal gas, pressure reads

$$p=(\gamma-1)\rho\left[E-\frac{u^2+v^2+w^2}{2}\right] \qquad (5)$$

and temperature is computed using equation of state.

3. SPATIAL DISCRETIZATION:

Discretization of the Euler equations in integral form is obtained by subdividing the computational domain Ω into separate hexahedral finite volumes Ω_{ijk} (i = 1,2,…,N_i, and j = 1,2,…, N_j) and by requiring the conservation laws for each finite volume separately. For a particular 2D control volume whose volume does not change with time, equation (1) becomes

$$\frac{d\vec{W}_{I,J}}{dt}=-\frac{1}{\Omega_{I,J}}\left[\sum_{m=1}^{NF}(\vec{F}_c\Delta S)_m\right] \qquad (6)$$

I, J address the particular control volume and NF denotes the number of control volume faces. ΔS_m denotes the area of the face m. After writing the equation (6) for all control volumes, a system of ODE of first order (which can be solved by advancing in time starting from a known initial solution and providing suitable BC's for inviscid fluxes) is obtained. Steady solution can be reached iteratively:

$$\vec{W}_{I,J}^{\,n+1}=\vec{W}_{I,J}^{\,n}-\frac{\Delta t}{\Omega_{I,J}}\vec{R}_{I,J} \qquad (7)$$

where $\vec{R}_{I,J}=\left[\sum_{m=1}^{NF}\left(\vec{F}_c-\vec{F}_V\right)_m\Delta S_m\right]$.

$\vec{R}_{I,J}$ is called the "residual". The finite volume discretization requires an evaluation of the convective fluxes at each cell face. In this work, convective fluxes are evaluated using central scheme of JST [1], and upwind schemes of Roe's approximate Riemann solver [2], and CUSP scheme [3].

Jameson-Schmidt-Turkel (JST) Scheme:

In this scheme, convective flux at the cell faces was computed from the arithmetic average of the conservative variables on both sides of the face. However, it allows for odd-even decoupling of the solution and overshoots at shocks. These drawbacks were overcome by adding artificial dissipation for stability. This scheme is first implemented for Euler equations by Jameson et al. [1]. It is less accurate in the resolution of boundary layers and shocks in comparison to upwind schemes. However, it is computationally cheaper. Total convective flux at cell face reads

$$\left(\vec{F}_c\Delta S\right)_{I+1/2,J}=\vec{F}_C\left(\vec{W}_{I+1/2,J}\right)\Delta S_{I+1/2,J}-\vec{D}_{I+1/2,J} \qquad (8)$$

where $\vec{W}_{I+1/2,J}=\frac{1}{2}\left(\vec{W}_{I,J}+\vec{W}_{I+1,J}\right)$, (9)

$$\vec{D}_{I+1/2}=\hat{\Lambda}^S_{I+1/2}[\varepsilon^{(2)}_{I+1/2}\left(\vec{W}_{I+1}-\vec{W}_I\right) -\varepsilon^{(4)}_{I+1/2}\left(\vec{W}_{I+2}-3\vec{W}_{I+1}+3\vec{W}_I-\vec{W}_{I-1}\right)]. \qquad (10)$$

The dissipation $\left(\vec{D}_{I+1/2}\right)$ is scaled by the sum of the spectral radii of the convective flux Jacobians:

$$\hat{\Lambda}^S_{I+1/2} = \frac{1}{2}\left[\left(\hat{\Lambda}^I_c\right)_I + \left(\hat{\Lambda}^I_c\right)_{I+1}\right] + \frac{1}{2}\left[\left(\hat{\Lambda}^J_c\right)_I + \left(\hat{\Lambda}^J_c\right)_{I+1}\right] \quad (11)$$

where $\hat{\Lambda}_c = (|V| + c)\Delta S$. V is the contravariant velocity and c is the speed of sound. The coefficients are computed as

$$\varepsilon^{(2)}_{I+1/2} = k^{(2)} \max(\chi_I, \chi_{I+1}) \quad (12)$$

$$\varepsilon^{(4)}_{I+1/2} = \max\left[0, \left(k^{(4)} - \varepsilon^{(2)}_{I+1/2}\right)\right]$$

with the pressure sensor given as

$$\chi_I = \frac{|p_{I+1} - 2p_I + p_{I-1}|}{p_{I+1} + 2p_I + p_{I-1}}. \quad (13)$$

$k^{(2)} = 1/2$ and $1/128 \le k^{(4)} \le 1/64$ are typical values.

Roe's Approximate Riemann Solver:

Roe approximate Riemann solver is based on the decomposition of the flux difference over a face of the control volume into a sum of wave contributions. Not only the direction of wave propagation, but also the waves themselves are considered. The convective fluxes at the face of a control volume from the left and right state are evaluated by solving the Riemann problem. The idea was first introduced by Godunov [7]. Since the Euler equations are non-linear, the corresponding Riemann problem is non-linear as well. This can be expensive to calculate in some cases, and Roe [2] found out that a properly selected approximate problem does the same job as well and reduces the computational effort considerably. Roe's method is popular due to its high accuracy for boundary layers and good resolution of shocks. Total convective flux at the face of a control volume reads [2, 8]

$$\left(\vec{F}_c\right)_{I+1/2,J} = \frac{1}{2}\left[\vec{F}_c\left(\vec{W}_R\right) + \vec{F}_c\left(\vec{W}_L\right)\right] - \frac{1}{2}\left[\left|\overline{A}_{Roe}\right|_{I+1/2,J}\left(\vec{W}_R - \vec{W}_L\right)\right] \quad (14)$$

where

$$\left|\overline{A}_{Roe}\right|\left(\vec{W}_R - \vec{W}_L\right) = \left|\Delta\vec{F}_1\right| + \left|\Delta\vec{F}_{2,3,4}\right| + \left|\Delta\vec{F}_5\right| \quad (15)$$

$$\left|\Delta\vec{F}_1\right| = \left|\widetilde{V} - \widetilde{c}\right|\left(\frac{\Delta p - \widetilde{\rho}\widetilde{c}\Delta V}{2\widetilde{c}^2}\right)\begin{bmatrix} 1 \\ \widetilde{u} - \widetilde{c}n_x \\ \widetilde{v} - \widetilde{c}n_y \\ \widetilde{w} - \widetilde{c}n_z \\ \widetilde{H} - \widetilde{c}\widetilde{V} \end{bmatrix}$$

$$\left|\Delta\vec{F}_{2,3,4}\right| = \left|\widetilde{V}\right|\left\{\left(\Delta p - \frac{\Delta\rho}{\widetilde{c}^2}\right)\begin{bmatrix} 1 \\ \widetilde{u} \\ \widetilde{v} \\ \widetilde{w} \\ \widetilde{q}^2/2 \end{bmatrix}\right\} + \widetilde{\rho}\left|\widetilde{V}\right|\begin{bmatrix} 0 \\ \Delta u - \Delta V n_x \\ \Delta v - \Delta V n_y \\ \Delta w - \Delta V n_z \\ \widetilde{u}\Delta u + \widetilde{v}\Delta v + \widetilde{w}\Delta w - \widetilde{V}\Delta V \end{bmatrix}$$

$$\left|\Delta\vec{F}_5\right| = \left|\widetilde{V} + \widetilde{c}\right|\left(\frac{\Delta p - \widetilde{\rho}\widetilde{c}\Delta V}{2\widetilde{c}^2}\right)\begin{bmatrix} 1 \\ \widetilde{u} + \widetilde{c}n_x \\ \widetilde{v} + \widetilde{c}n_y \\ \widetilde{w} + \widetilde{c}n_z \\ \widetilde{H} + \widetilde{c}\widetilde{V} \end{bmatrix}.$$

Roe-averaged variables are computed from the left and left state by the formulae

$$\widetilde{\rho}_{I+1/2} = \sqrt{\rho_R \rho_L}$$

$$\widetilde{u}_{I+1/2} = \frac{\sqrt{\rho_R}u_R + \sqrt{\rho_L}u_L}{\sqrt{\rho_R} + \sqrt{\rho_L}}$$

$$\widetilde{v}_{I+1/2} = \frac{\sqrt{\rho_R}v_R + \sqrt{\rho_L}v_L}{\sqrt{\rho_R} + \sqrt{\rho_L}}$$

$$\widetilde{H}_{I+1/2} = \frac{\sqrt{\rho_R}H_R + \sqrt{\rho_L}H_L}{\sqrt{\rho_R} + \sqrt{\rho_L}} \quad (16)$$

$$\widetilde{c}_{I+1/2} = \sqrt{(\gamma - 1)\left(\widetilde{H} - \frac{\widetilde{u}^2 + \widetilde{v}^2}{2}\right)}_{I+1/2}$$

$$\widetilde{V}_{I+1/2} = \widetilde{u}_{I+1/2}n_x + \widetilde{v}_{I+1/2}n_y$$

The jump condition is defined as $\Delta(\bullet) = (\bullet)_R - (\bullet)_L$.

The original scheme does not recognise the sonic point. This problem was overcome by modifying the modulus of the eigenvalues $|\Lambda_c| = |\widetilde{V} \pm \widetilde{c}|$ using Harten's entropy correction [9].

$$|\Lambda_c| = \begin{cases} |\Lambda_c| & if\ |\Lambda_c| \ge \delta \\ \dfrac{\Lambda_c^2 + \delta^2}{2\delta} & if\ |\Lambda_c| \le \delta \end{cases} \quad (17)$$

where $\delta \approx O(\widetilde{c}/10)$.

Convective Upwind Split Pressure Scheme:

This scheme was introduced by Jameson [3, 10, and 11] and modified by Tatsumi, Martinelli, and Jameson [12]. It belongs to a family of schemes based on a splitting of the flux vector into convective and pressure flux contributions. The CUSP scheme has several advantages. First, it can be considered as a type of artificial viscosity, since it is defined as a sum of the central flux average plus a dissipative flux. Hence, it can be used with a various time-stepping schemes. Second, the CUSP formulation can be used with multistage schemes which do not evaluate the artificial dissipation fluxes at every stage, in order to reduce computational work. Another advantage of the CUSP scheme is that it can be easily combined with preconditioning, since preconditioning is based on the

inviscid flux form and not the artificial dissipation. The CUSP scheme is specifically developed for oscillation-free, single-interior-point shock capturing, and also provides low dissipation for low Mach numbers. Total convective flux at the face of a control volume is computed as

$$\left(\vec{F}_C\right)_{I+1/2}=\frac{1}{2}\left[\vec{F}_C\left(\vec{W}_R\right)+\vec{F}_C\left(\vec{W}_L\right)\right]-\vec{D}_{I+1/2} \tag{18}$$

The dissipation term includes a linear combination of the differences of the state and the flux vector.

$$\vec{D}_{I+1/2}=\frac{1}{2}\left(\alpha^* c\right)_{I+1/2}\left\{\begin{bmatrix}\rho\\ \rho u\\ \rho v\\ \rho w\\ \rho H\end{bmatrix}_R-\begin{bmatrix}\rho\\ \rho u\\ \rho v\\ \rho w\\ \rho H\end{bmatrix}_L\right\}+ \tag{19}$$

$$\frac{1}{2}\beta_{I+1/2}\left\{\begin{bmatrix}\rho V\\ \rho uV+n_x p\\ \rho vV+n_y p\\ \rho wV+n_z p\\ \rho HV\end{bmatrix}_R-\begin{bmatrix}\rho V\\ \rho uV+n_x p\\ \rho vV+n_y p\\ \rho wV+n_z p\\ \rho HV\end{bmatrix}_L\right\}$$

The above formulation is called HCUSP scheme, since the total enthalpy is preserved [13]. The two parameters α^* and β are defined as

$$\alpha^* c=\begin{cases}\left|\widetilde{V}\right| & \text{if } \beta=0\\ -(1+\beta)\Lambda^- & \text{if } \beta>0 \text{ and } 0<\mathrm{M_n}<1\\ +(1-\beta)\Lambda^+ & \text{if } \beta<0 \text{ if } -1<\mathrm{M_n}<0\\ 0 & \text{if } |M_n|\geq 1\end{cases} \tag{20}$$

$$\beta=\begin{cases}+\max\left(0,\dfrac{\widetilde{V}+\Lambda^-}{\widetilde{V}-\Lambda^-}\right) & \text{if } 0\leq \mathrm{M_n}<1\\ -\max\left(0,\dfrac{\widetilde{V}+\Lambda^+}{\widetilde{V}-\Lambda^+}\right) & \text{if } -1\leq \mathrm{M_n}<0\\ \mathrm{sgn}(M_n) & \text{if } |M_n|\geq 1\end{cases} \tag{21}$$

where $M_n=\widetilde{V}/\widetilde{c}$ and the positive and negative eigenvalues are given as

$$\Lambda^{\pm}=\frac{\gamma+1}{2\gamma}\widetilde{V}\pm\sqrt{\left(\frac{\gamma-1}{2\gamma}\widetilde{V}\right)^2+\frac{\widetilde{c}^{\,2}}{\gamma}} \tag{22}$$

where $\widetilde{V}$ is the contravariant velocity, γ is the specific heat coefficient, and $\widetilde{c}$ is the speed of sound. All flow variables in equations 18-20 are obtained at the cell faces using Roe averages [2, 8].

In upwind schemes, left and right states are evaluated using MUSCL approach [5], which reads

$$\begin{aligned}U_R&=U_{I+1}-\frac{1}{2}\Psi_R\left(U_{I+2}-U_{I+1}\right)\\ U_L&=U_I-\frac{1}{2}\Psi_L\left(U_I-U_{I-1}\right)\end{aligned} \tag{23}$$

where $\Psi_{L/R}=\dfrac{1}{2}\left[(1+\hat{\kappa})r_{L/R}+(1-\hat{\kappa})\right]\Phi_{L/R}$. (24)

In the above formulations, Φ is slope limiter and Ψ is the limiter function. For $\hat{\kappa}=0$; selecting $\Phi(r)=\dfrac{2r}{r^2+1}$ and $\Psi(r)=\dfrac{r^2+r}{1+r^2}$ corresponds to Van Albada Limiter [6]. Hence, MUSCL interpolation gives

$$\begin{aligned}U_R&=U_{I+1}-\frac{1}{2}\left[\frac{a\left(b^2+\varepsilon\right)+b\left(a^2+\varepsilon\right)}{a^2+b^2+2\varepsilon}\right]\\ U_L&=U_I+\frac{1}{2}\left[\frac{a\left(b^2+\varepsilon\right)+b\left(a^2+\varepsilon\right)}{a^2+b^2+2\varepsilon}\right]\end{aligned} \tag{25}$$

where $\begin{matrix}a_R=U_{I+2}-U_{I+1}\\ a_L=U_{I+1}-U_I\end{matrix}$, and $\begin{matrix}b_R=U_{I+1}-U_I\\ b_L=U_I-U_{I-1}\end{matrix}$.

The parameter ε prevents the activation of the limiter in smooth flow regions due to small scale oscillations [14].

4. TEMPORAL DISCRETIZATION:

For steady problems with cell-centered discretization, basic explicit scheme is written as

$$\Delta\vec{W}_I^{\,n}=-\frac{\Delta t_I}{\Omega_I}\vec{R}_I^{\,n} \tag{26}$$

For five stage hybrid scheme, where the dissipative terms are evaluated at odd stages, the spatial discretization is split into two parts

$$\vec{R}_I=\left(\vec{R}_c\right)_I-\left(\vec{R}_d\right)_I \tag{27}$$

The first part contains discretization of the convective fluxes. The second part is composed of the numerical dissipation.

$$\begin{aligned}\left(\vec{R}_c\right)_I&=\sum_{k=1}^{N_F}\left[\vec{F}_c\left(\vec{W}_{I+1/2}\right)\Delta S\right]_k\\ \left(\vec{R}_d\right)_I&=\sum_{k=1}^{N_F}\left[\vec{D}\right]_k\end{aligned} \tag{28}$$

Then, the hybrid multistage scheme reads

$$\begin{aligned}\vec{W}_I^{(0)}&=\vec{W}_I^{\,n}\\ \vec{W}_I^{(1)}&=\vec{W}_I^{(0)}-\alpha_1\frac{\Delta t_I}{\Omega_I}\left[\vec{R}_c^{(0)}-\vec{R}_d^{(0)}\right]_I\\ \vec{W}_I^{(2)}&=\vec{W}_I^{(0)}-\alpha_2\frac{\Delta t_I}{\Omega_I}\left[\vec{R}_c^{(1)}-\vec{R}_d^{(0)}\right]_I\\ \vec{W}_I^{(3)}&=\vec{W}_I^{(0)}-\alpha_3\frac{\Delta t_I}{\Omega_I}\left[\vec{R}_c^{(2)}-\vec{R}_d^{(2,0)}\right]_I\\ \vec{W}_I^{(4)}&=\vec{W}_I^{(0)}-\alpha_4\frac{\Delta t_I}{\Omega_I}\left[\vec{R}_c^{(3)}-\vec{R}_d^{(2,0)}\right]_I\end{aligned} \tag{29}$$

$$\vec{W}_I^{(n+1)} = \vec{W}_I^{(0)} - \alpha_5 \frac{\Delta t_I}{\Omega_I}\left[\vec{R}_c^{(4)} - \vec{R}_d^{(4,2)}\right]_I$$

where

$$\vec{R}_d^{(2,0)} = \beta_3 \vec{R}_d^{(2)} + (1-\beta_3)\vec{R}_d^{(0)}$$
$$\vec{R}_d^{(4,2)} = \beta_5 \vec{R}_d^{(4)} + (1-\beta_5)\vec{R}_d^{(2,0)} \quad (30)$$

Table 1 presents stage coefficients α_m and blending coefficients β_m for central and upwind schemes in case of (5-3) hybrid scheme.

The basic explicit time-stepping scheme is further accelerated by local time stepping and implicit residual smoothing (IRS). With local time stepping, the solution at each cell is advanced at the maximum Δt allowed by the stability. Implicit smoothing of residuals is used to extend the stability range of the basic scheme.

Table 1. Hybrid Multistage scheme

	Central scheme		Upwind Scheme	
Stage	α	β	α	β
1	0.2500	1.00	0.2742	1.00
2	0.1667	0.00	0.2067	0.00
3	0.3750	0.56	0.5020	0.56
4	0.5000	0.00	0.5142	0.00
5	1.0000	0.44	1.0000	0.44

Jameson and Baker [15] first introduced the residual smoothing technique with the aim to give the explicit scheme an implicit character. Maximum allowable CFL number is increased considerably. IRS reads

$$-\varepsilon^I \vec{R}^*_{I-1,J} + (1+2\varepsilon^I)\vec{R}^*_{I,J} - \varepsilon^I \vec{R}^*_{I+1,J} = \vec{R}_{I,J} \quad (31)$$
$$-\varepsilon^J \vec{R}^{**}_{I,J-1} + (1+2\varepsilon^J)\vec{R}^{**}_{I,J} - \varepsilon^J \vec{R}^{**}_{I,J+1} = \vec{R}^*_{I,J}$$

where $\vec{R}^*_{I,J}$, $\vec{R}^{**}_{I,J}$ denote the residuals in I, J directions. Smoothing coefficients read [12]

$$\varepsilon^I = \max\left\{\frac{1}{4}\left[\left(\frac{\sigma^*}{\sigma}\frac{1}{1+\Psi r^J}\right)^2 - 1\right], 0\right\} \quad (32)$$
$$\varepsilon^J = \max\left\{\frac{1}{4}\left[\left(\frac{\sigma^*}{\sigma}\frac{1}{1+\Psi r^I}\right)^2 - 1\right], 0\right\}$$

$\Psi = 0.125$ is taken. The maximum ratio of the CFL numbers of the smoothed and unsmoothed scheme is dependent on the value of the smoothing coefficient,

$$\frac{\sigma^*}{\sigma} \le \sqrt{1+4\varepsilon} \quad (33)$$

The ratios of the convective spectral radii read

$$r^I = \frac{\hat{\Lambda}^J_C}{\hat{\Lambda}^I_C} \text{ and } r^J = \frac{\hat{\Lambda}^I_C}{\hat{\Lambda}^J_C} \quad (34)$$

5. BOUNDARY CONDITIONS:

Boundary conditions were treated by using two layers of ghost cells, which are built by extending the discretization stencil beyond the computational boundaries. At the solid, adiabatic wall, flow tangency is maintained and the wall pressure is obtained by extrapolation from the interior domain. Symmetry plane is treated by using the concept of reflected cells, which means that flow variables in the ghost cells are set equal to neighboring interior cells. Inflow/outflow boundary conditions, which are based on the Riemann invariants corresponding to the incoming and outgoing waves, were implemented to the rest of the boundaries.

6. COMPUTATIONAL RESULTS:

The numerical results given here demonstrate the accuracy and computational efficiency of the studied schemes for internal flows in a channel with a circular bump on the lower wall. The computations with 33x9 (coarse), 65x17 (fine), and 129x33 (finer) grid points were carried out to determine grid independent solution. Computed results agree well with the ones in reference [16]. Figure 1 presents the computational mesh, which includes 65x17 grid points, used in all computations. The width of the channel is equal to the length of the bump and the thickness-to-chord ratio of the bump is 10%. This geometry is identical to the test case used in reference [17]. For all computations, the flow in a channel was initially uniform having the far upstream properties. The solution was assumed to reach the steady state when the average absolute correction of normalized density is less than 1x10-5. CFL value of 2.5 is utilized. All computations were performed on a PC including 512 Mb memory and 2 GHz CPU running Windows XP.

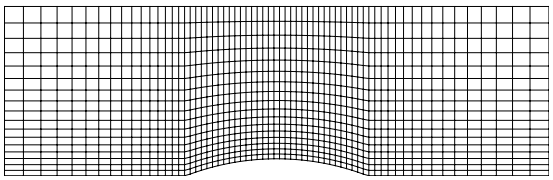

Figure 1. Fine computational mesh.

Table 2. Computational work.

Mach	Grid Density	JST	CUSP	ROE
	33x9	✓	✓	✓
0.5	65x17	✓	✓	✓
	129x33	✓	✓	✓
	33x9	✓	✓	✓
0.675	65x17	✓	✓	✓
	129x33	✓	✓	✓
1.4	65x17	✓	✓	✓

Table 3. Computational performance (M=0.5).

	Grid Density	JST	CUSP	ROE
CPU time (Sec.)	33x9	52	68	48
	65x17	921	1320	1196
	129x33	7680	9490	8630
Memory (Mb.)	33x9	1.3	1.4	1.4
	65x17	1.6	1.7	1.7
	129x33	1.9	2.0	2.0

Table 2-5 present the computational work done in this study. As expected, JST scheme was observed to be computationally cheaper than upwind schemes in all flow cases.

Table 4. Computational performance (M=0.675).

	Grid Density	JST	CUSP	ROE
CPU time (Sec.)	33x9	14	31	29
	65x17	90	177	167
	129x33	796	1440	1400
Memory (Mb.)	33x9	1.3	1.4	1.4
	65x17	1.6	1.7	1.7
	129x33	1.9	2.0	2.0

Table 5. Computational performance (M=1.4).

	Grid Density	JST	CUSP	ROE
CPU time (Sec.)	65x17	26	85	60
Memory (Mb.)	65x17	1.6	1.7	1.7

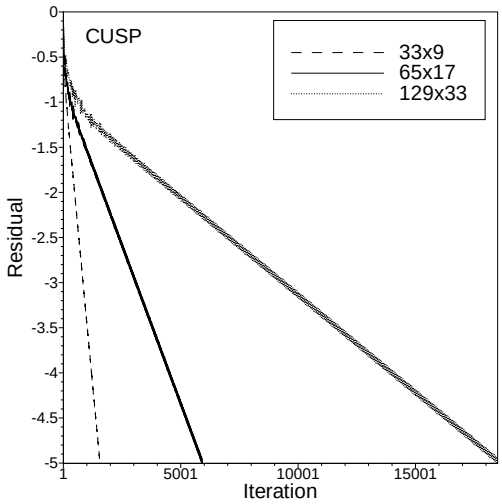

Figure 2. Typical convergence history, M=0.5

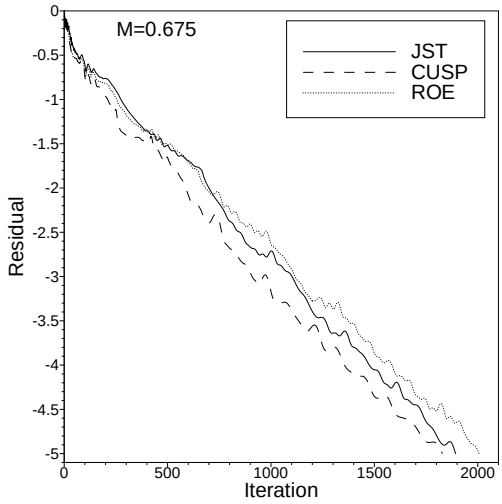

Figure 3. Convergence history of available schemes

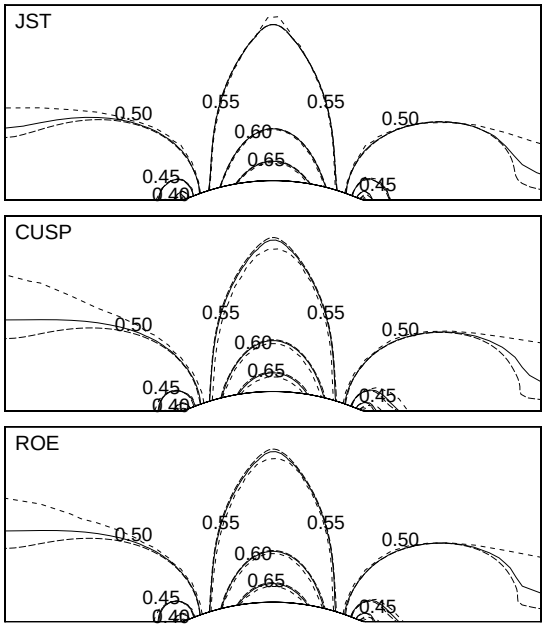

Figure 4. Grid sensitivity, M=0.5

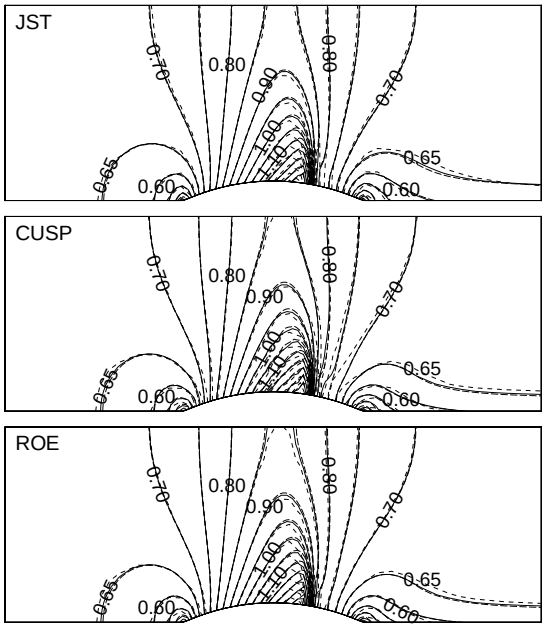

Figure 5. Grid sensitivity, M=0.675

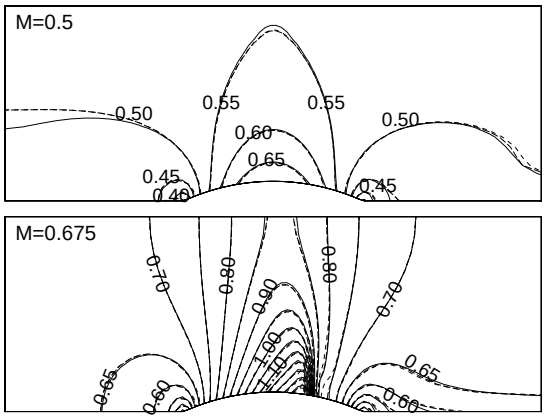

Figure 6. Isomach contours for available schemes

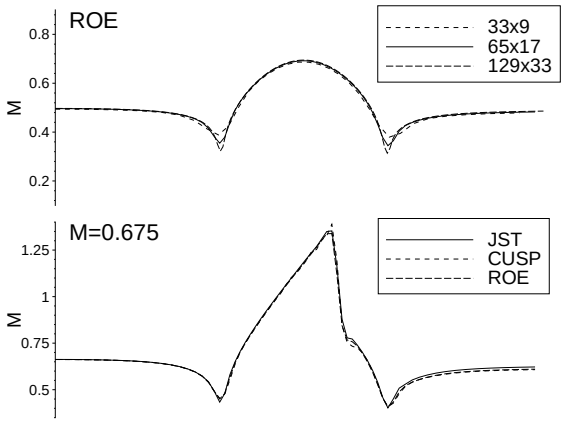

Figure 7. Mach number distribution

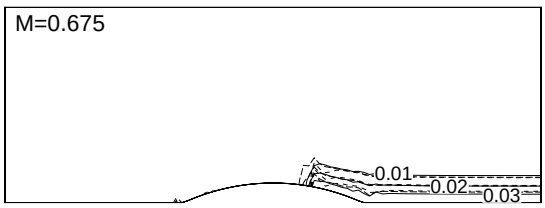

Figure 8. Total pressure loss contours

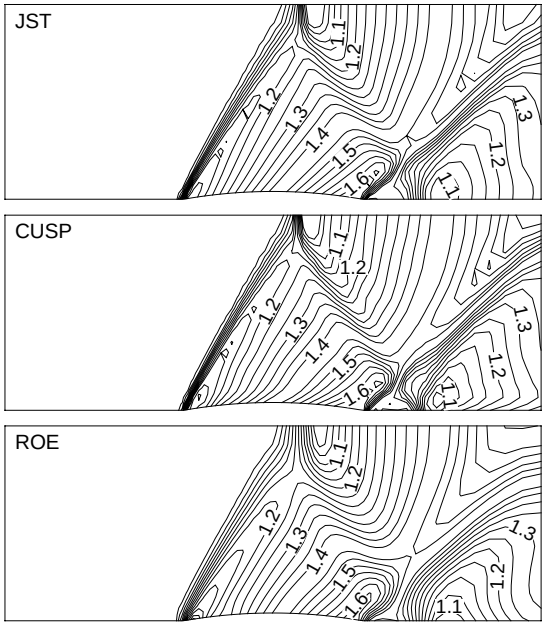

Figure 9. Isomach contours for available schemes

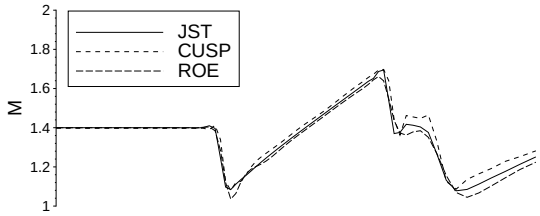

Figure 10. Mach number distribution, M=1.4

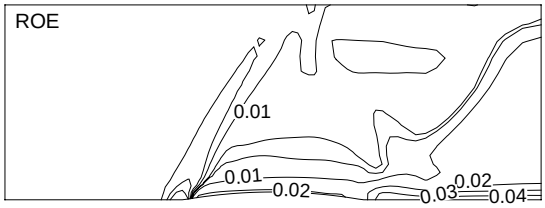

Figure 11. Total pressure loss contours, M=1.4

Figure 2 presents typical convergence histories for three grid densities. For this subsonic (M=0.5) case, the errors reflecting back and forth in the solution domain slow down the convergence. Coarsening the grid size allows better damping of errors, which results in faster convergence to steady state. Figure 3

presents typical convergence histories for available schemes for transonic (M=0.675) case. All schemes have similar convergence rate.

Figure 4-5 present solutions for subsonic and transonic flow cases with three grid densities. Solid, dashed, and long dashed lines represent the solutions computed using fine, coarse, and finer grids respectively. Fine and finer grids yield similar solutions, which is an indication of grid independent solution. Figure 6 presents the solutions computed using JST (solid line), CUSP (dashed line), and ROE (long dashed line) schemes with fine grid. The solution is quite symmetric about the midchord, which is a good indication of accuracy for the subsonic application. Upwind schemes yield quite similar results, which also agree well with that of JST scheme. In the solution at M=0.675, a supersonic region, which is terminated by shock, appears. The captured shock is located at around 72% of chord and it is spread over three grid points in JST scheme. The shocks, captured by upwind schemes, are similar to each other and are sharper in comparison to that of JST scheme (Figure 7). The flow behind the shock is rotational and thus the isomach lines downstream of the shock no longer intersect the lower wall at right angles. Figure 8 shows the total pressure loss $-\Delta p_T = 1.0 - (p_T / p_{T-\infty})$- contours for transonic case. The loss reaches to its maximum value at the middle shock point. The lines of constant loss behind the shock follow the streamlines, which is an expected result for an inviscid rotational flow.

Figure 9-11 present the solutions for supersonic (M=1.4) case. Two oblique shocks are formed at the leading and trailing edge of the bump. The leading edge shock is dissipated by the expansion waves transmitted from the bump surface at the downstream. The shock is spread over about five grid cells at the symmetry plane and reflected back to the expansion region, where it is dissipated. The trailing edge shock is also dissipated by the upstream expansion waves and leaves the computational domain.

7. CONCLUSION:

The present two dimensional Euler solver based on cell-centered finite volume discretization technique with central scheme of JST, and upwind schemes of Roe's approximate Riemann solver and CUSP scheme works efficiently for internal flows at subsonic, transonic, and supersonic speeds. For upwind schemes, MUSCL approach, which is enhanced by using Van Albada Limiter in order to suppress the non-physical oscillations of the solution, works well. The convergence of the basic explicit time stepping scheme is successfully accelerated by applying local time-stepping and implicit residual smoothing techniques.

Numerical results agree well with that of available in the open literature and they indicate that present solver is accurate, and reliable for predicting inviscid rotational, and/or irrotational flows. In comparison to central scheme, upwind schemes are superior in capturing strong gradients present in the flow domain. However, they require more CPU time and computational memory. All schemes yield good convergence rates for a wide range of flow speeds. Further improvement to current solver for handling external flows will provide a valuable numerical tool for aerodynamic applications as well. Evaluation of diffusive fluxes will improve the reliability and flexibility of the solver as an engineering tool for handling viscous flows as well.

7. ACKNOWLEDGMENT:

The first author wishes to thank Dr. Rustem Arslan and Dr. Fırat E. Oğuz of Aeronautical Engineering Department. at Technical University of Istanbul for their discussions.

8. REFERENCES:

[1] Jameson, A., Schmidt, W., Turkel, E., 1981, "Numerical Solutions of the Euler Equations by Finite Volume Methods Using Runge-Kutta Time-Stepping Schemes," AIAA Paper 81-1259.

[2] Roe, P.L., 1981, "Approximate Riemann Solvers, Parameter Vectors, and Difference Schemes," Journal of Computational Physics, 43: 357-372.

[3] Jameson, A., 1993, "Artificial Diffusion, Upwind Biasing, Limiters and Their Effect on Accuracy and Multigrid Convergence in Transonic and Hypersonic Flow," AIAA Paper 93-3559.

[4] Warming, R.F., and Beam, R.W., 1976, "Upwind Second Order Difference Schemes and Applications in Aerodynamic Flows," AIAA Journal, Vol. 24, pp. 1241-1249.

[5] Leer, B. V., 1977, "Towards the Ultimate Conservation Difference Scheme IV; A New Approach to Numerical Convection," Journal of Computational Physics, 23: 276-299.

[6] Albada, G.D., Leer, B. V., and Roberts, W.W., 1982, "A Comparative Study of Computational Methods in Cosmic Gas Dynamics," Astron. Astrophysics, 108:76-84.

[7] Godunov, S.K., 1959, "A difference Scheme for Numerical Computation Discontinuous Solution of Hydrodynamic Equations," Math. Sbornik (in Russian), 47, pp. 271-306.

[8] Roe, P.L.; Pike, J., "Efficient Construction and Utilization of Approximate Riemann Solutions," Computing Methods in Applied Sciences and Engineering, R. Glowinski, J.L. Lions (eds.),

North Holland Publishing, The Netherlands, 1984.

[9] Harten, A., Lax, P.D., Van Leer, B., 1983, "On Upstream Differencing and Godunov-Type Schemes for Hyperbolic Conservation Laws," Soc. Indust. and Appl. Math. Rev., 25, No.1.

[10] Jameson, A., 1995, "Positive Schemes and Shock Modeling for Compressible Flows," Inter. J. Numerical Methods Engineering, 20:743-776.

[11] Jameson, A., 1995, "Analysis and Design of Numerical Schemes for Gas Dynamics II: Artificial Diffusion and Discrete Shock Structure," Int. J. Computational Fluid Dynamics, Vol. 5, pp. 1-38.

[12] Tatsumi, S., Martinelli, L. and Jameson, 1994, "A Design, Implementation and Validation of Flux Limited Schemes for the Solution of the Compressible Navier-Stokes Equations," AIAA Paper 94-0647.

[13] Tatsumi, S., Martinelli, L., Jameson, A., 1995, "A New High Resolution Scheme for Compressible Viscous Flow with Shocks," AIAA Paper 95-0466.

[14] Venkatakrishnan, V., 1993, "On the Accuracy of Limiters and Convergence to Steady State Solutions," AIAA Paper 93-0880

[15] Jameson, A., Baker, T.J., 1983, "Solution of the Euler Equations for Complex Configurations," AIAA paper 83-1929.

[16] Rho-Ho, Ni, 1982, "A Multiple Grid Scheme For Solving the Euler Equations," AIAA Journal, Vol. 20, No. 11.

[17] Moretti, G., 1981, "Experiments on Initial and Boundary Conditions," Paper Presented At Symposium on Numerical and Physical Aspects of Aerodynamic Flow.

VITA

Capt. Murat UYGUN

He was graduated from Aeronautical Engineering Department at Turkish Air Force Academy, Istanbul in August 1995. He received his M.Sc. degree in Aerospace Engineering from Middle East Technical University, Ankara in September 2000. Later, he joined Aeronautical Engineering Department at Turkish Air Force Academy, Istanbul. His thesis and follow-on work as a PhD student in Mechanical Engineering at Istanbul Technical University, involves numerical simulation of internal and external viscous flow fields. During 2002-2003, he conducted a study on *Generic Scripted Grid Generation* as a NATO Fellow at Defence Research Development Canada-Atlantic (DRDC-Atlantic), Halifax, Canada. His current research interests are Computational Fluid Dynamics, Upwind-Finite Volume schemes, compressible flows, low Mach number preconditioning, convergence acceleration techniques, and turbulence modeling. He is a member of American Institute of Aeronautics and Astronautics (AIAA).

Prof.Dr. Kadir KIRKKÖPRÜ

He obtained his BS and MSc degrees from Mechanical Engineering Department at Istanbul Technical University (ITU) in 1979 and 1981, respectively. He received his PhD degree in Mechanical Engineering from the University of Colorado (CU) at Boulder in 1988. He was Senior Research Associate in Mathematics and Physics Department at the University of East Anglia in England between 1988 and 1990. He joined Mechanical Engineering Department at ITU in 1990. Later, he worked in the Applied Mathematics Department at CU Boulder for two years. He has been professor in Mechanical Engineering Department at ITU since 1998. His main research interests are Analytical and Computational Fluid Dynamics, Fluid Machinery, Asymptotic Techniques and Theoretical Combustion.